



**HAL**  
open science

## Improvement of safety, longevity and performance of lead acid battery in off-grid PV systems

Bachirou Bogno, Jean-Paul Sawicki, Takla Salame, Michel Aillerie, Frédéric Saint-Eve, Oumarou Hamandjoda, Beda Tibi

### ► To cite this version:

Bachirou Bogno, Jean-Paul Sawicki, Takla Salame, Michel Aillerie, Frédéric Saint-Eve, et al.. Improvement of safety, longevity and performance of lead acid battery in off-grid PV systems. *International Journal of Hydrogen Energy*, 2017, 42 (5), pp.3466 - 3478. 10.1016/j.ijhydene.2016.12.011 . hal-01519731

**HAL Id: hal-01519731**

**<https://centralesupelec.hal.science/hal-01519731v1>**

Submitted on 17 Mar 2022

**HAL** is a multi-disciplinary open access archive for the deposit and dissemination of scientific research documents, whether they are published or not. The documents may come from teaching and research institutions in France or abroad, or from public or private research centers.

L'archive ouverte pluridisciplinaire **HAL**, est destinée au dépôt et à la diffusion de documents scientifiques de niveau recherche, publiés ou non, émanant des établissements d'enseignement et de recherche français ou étrangers, des laboratoires publics ou privés.

# Improvement of safety, longevity and performance of lead acid battery in off-grid PV systems

Bachirou Bogno<sup>a,b,c,d</sup>, Jean-Paul Sawicki<sup>b,c</sup>, Takla Salame<sup>b,c,e</sup>,  
Michel Aillerie<sup>b,c,\*</sup>, Frédéric Saint-Eve<sup>b,c</sup>, Oumarou Hamandjoda<sup>d</sup>,  
Beda Tibi<sup>d</sup>

<sup>a</sup> University of Maroua, P.O. Box 46, Maroua, Cameroon

<sup>b</sup> Université de Lorraine, LMOPS-EA 4423, 57070, Metz, France

<sup>c</sup> CentraleSupélec, LMOPS, 57070, Metz, France

<sup>d</sup> University of Yaoundé I, ENSP, P.O. Box 8390, Yaoundé, Cameroon

<sup>e</sup> CEER, Faculty of Sciences II, Lebanese University, B.P 90656, Jdeidet El Mten, Lebanon

---

## ARTICLE INFO

### Article history:

Received 25 October 2016

Received in revised form

2 December 2016

Accepted 3 December 2016

Available online xxx

### Keywords:

Off-grid PV systems

Lead acid battery

Three-Stage Charging control

MPPT charge controller

---

## ABSTRACT

In a renewable energy system, in order to ensure continuous production, batteries associated to a charge controller are always necessary whenever the source of charging is solar, wind, or hydraulics. For photovoltaic (PV) systems, an excessive energy produced by solar cells during intense sunlight peak conditions could damage the batteries. A charge controller is therefore used to maintain the suitable charging voltage to the batteries so that, as the input voltage from the PV module rises, the charge controller regulates the process, thus, preventing any overcharging. This paper presents a practical solution for off-grid PV systems using standard commercial elements. A detailed analysis is carried out based on experimental results of the battery charge control allowing a long-life and a high safety of the autonomous storage and production systems. The experimental work was performed with a solar battery (24 V-55 Ah) charged by a 175Wp PV module, through a Maximum-Power-Point-Tracking/Three-Stage-Charging-Cycle (MPPT/TSCC) charge controller. The benefits of the Three-Stage-Charging-Cycle (TSCC) control as well as the Maximum-Power-Point-Tracking (MPPT) have been thus proven for the efficiency of the recharge, both qualitatively and quantitatively.

---

## Introduction

Operating a power system from renewables, such as wind or solar, is constrained in many instances by the variable and intermittent nature of their inputs and output. This calls for practical application and management of energy-storage

systems [1]. One of the most promising, innovative and efficient solutions of electrical energy storage is the solution based on integration of batteries directly in renewables power systems [2]. Within this solution, during low consumption period, the extra energy produced is stored in the battery and during peak consumption period or to compensate the intermittence of the renewable sources, the stored energy is used

---

\* Corresponding author. Université de Lorraine, LMOPS-EA 4423, 57070, Metz, France.

E-mail address: [aillerie@metz.supelec.fr](mailto:aillerie@metz.supelec.fr) (M. Aillerie).

<http://dx.doi.org/10.1016/j.ijhydene.2016.12.011>

to supply the energy demand. Batteries are commonly referred to as one of the weakest components in off-grid photovoltaic (PV) systems in the field and the criteria for the selection of solutions for the storage of renewable energy are still under debate [3,4]. A complex set of parameters has to be considered in the choice of the storage system being associated in the renewable power generator as technical, economic and environmental ones [5–8]. Hydrogen-based storage systems are sometimes coupled with renewable energy sources and a lot of study on possibilities of improving efficiency of electrolyzers coupled with renewables [9–13]. Nevertheless, more mature solutions associate photovoltaic panels or wind turbines with for renewables, standard or specially designed lead-acid batteries to store the intermittent produced energy in off-grid systems [14,15].

Usually, even in standard functioning conditions but worst when intermittent possibilities of charging are only possible, the lifetime of the storage elements is very often below expectations and therefore a regular replacement is required, which consequently increases the overall cost of the renewable energy sources [16,17]. The lifetime of a battery is not only influenced by the internal electrochemical and construction parameters, but also by operating parameters [18,19]. Therefore, battery management systems in PV applications have the task to operate the batteries at conditions that will not reduce their lifetime. Additionally, it is possible to maintain and optimize the performance, while increasing the lifetime of a battery by special operation regimes of charge and discharge.

Once in operation, any battery has to work within a controlled and limited power range in order to satisfy lifetime expectancy. Excessive overcharge and deep discharge conditions must be avoided by appropriate charge regulation, according to the battery type and characteristics. Compatibility between battery requirements and the associated charge controller seems to be, and is in practice, a decisive point to extend battery lifetime [17]. For lead acid batteries, whatever the type, most solar battery manufacturers recommend a Three-Stage-Charging-Cycle (TSCC) even if other technics exist [20–22]. Indeed, the TSCC represents the best and most efficient way to return full capacity to the battery and extend battery lifetime [14–18]. In fact, current battery charging

technologies, the so-called “smart chargers”, rely on micro-processors to recharge using three stages regulated charging: bulk, absorption, and float. Qualification or equalization is sometimes considered as another stage, a two-stage unit is bulk and float stages.

Charge control, therefore, clearly appears as a keystone of any autonomous PV system. The objective of this publication is to highlight the function of a MPPT/TSCC controller in the operation management of an off-grid system based on PV and batteries, not only for the control of safety limits of battery operating parameters (overcharge, deep discharge, ...) and self-discharge, but also for high energy efficiency both by reducing the fluctuation of the solar power and fitting the Maximum Power Point (MPP) voltage of the PV module to the battery charging voltage.

The experiment is conducted on a real PV system installation, and the charge controller is additionally featured with a tracker. Indeed, mainly two types of TSCC controllers stand out from others. Using traditional Pulse Width Modulation (PWM) charge controllers, the PV module is directly connected to the battery, which then sets the operating voltage. Therefore, charging power remains lower than if the controller was directly connected with the PV module. The use of MPPT charge controllers has many advantages, but the most relevant argument is certainly that it is increasingly difficult to find a suitable PV module for direct battery charging. Low cost grid injection PV modules are generally utilized, but these cannot be associated with a conventional controller because of their voltage. MPPT controllers yield at least 15% more power supply as compared to conventional PWM controllers [19,23–27]. The one used in the present work is the MPPT/TSCC Victron BlueSolar Charge Controller.

## Experimental set-up and methodology

The aim of this work is to experiment and analyze, in real operating conditions of off-grid PV systems, the charge control of a lead acid battery with a TSCC and MPPT charge controller. Fig. 1 shows the experimental setup of the study.

The PV module is taken from the actual installation of the experimental PV station of the laboratory, meeting the local

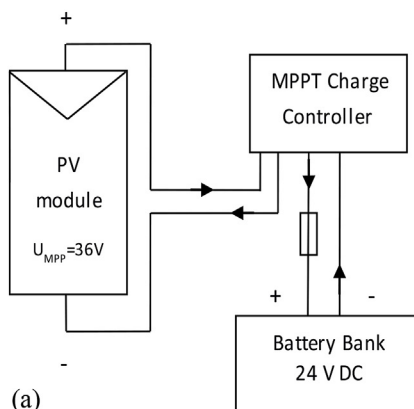


Fig. 1 – (a) Electrical scheme (b) A view of the experimental setup.

criteria (inclination and orientation) for best photovoltaic production. The battery bank is a series association of two 12 V-55 Ah AGM batteries to achieve a nominal voltage in accordance with the PV module. Measurement is instrumented by a data acquisition system monitored by a computer. This experiment finally allowed to fully recharging the battery bank, and then acquired measurements are computed and analyzed with Microsoft Excel software.

### The photovoltaic module

The PV module used in this experiment is taken from the solar roof of the laboratory. These are 16 identical monocrystalline silicon panels of 175 W each, interconnected in two groups of eight panels (2 strings of 4 and 8 other individual). Each group is connected to an individual inverter in the connection terminal for the electrical network injection. Our considered module is among the eight individually connected. Table 1 presents its technical specifications.

### The charge controller

The characteristics of the charge controller are given in Table 2.

### The battery bank

Due to the voltage provided by the PV module at MPP (36, 45 V) and the controller corresponding operating range of the MPPT (30–70 V), the battery bank is an association of two 12 V-55 Ah AGM batteries connected in series string to make a 24 V-55 Ah battery pack that can be charged with the 24 V output charge controller. Consequently, as for any batteries association,

some cautions have been taken to avoid accelerated aging of the associated batteries. Both batteries are identical (brand, reference, ampere) and purchased at the same time, about two years before experiments, so they have grown old together. Ideally, it should have the same charge density and have the same open-circuit voltage, but one can observe a slight open-circuit voltage difference (20 mV) when completely charged to 100%, since the beginning.

Because of constraints introduced by the data acquisition module connectors, we used cables of 2.5 mm<sup>2</sup> that turn out to be widely enough for the currents in presence (3–6 A).

### The data acquisition system

The acquisition of electrical measurements is instrumented using a data acquisition system monitored by a computer. This system is composed by a setting card of the four measurements performed simultaneously (voltage and current of the PV module upstream the charge controller, voltage and current of battery downstream); and an analog/digital conversion module (LabJack U3 LV module), Fig. 2.

Voltage measurement requires an opto-coupler associated with an operational amplifier whose gain is adjustable so as not to exceed the maximum allowable voltage for the analog inputs of the conversion module (2.44 V<sub>max</sub>). Current measurement is made by means of Hall sensors (LEM HSX 20-NP), the zero adjustment is accessible via a multi-turns resistance. In addition, as for voltage measurement it is possible to play on the gain of an operational amplifier so as not to exceed the allowable input voltage of the analog/digital conversion module.

The LabJack U3 LV module performs a conversion to 12 bits, which provides a very good measuring accuracy, with the risk nevertheless of being affected by the noise of the sensors. Yet we have chosen not to add additional filters to the interface card and signal conditioning.

### Data acquisition settings

The capture of signals is performed by means of a particularly simple handling software, ProfiLab-Expert 4.0 [28]. The programming of the “real time” measurements display and registration application is made by a “Functional Block Diagram” language type. The ProfiLab programming model of this instrumentation is shown in Fig. 3.

The calibration of the voltage and current sensors of the setting card was made using two multimeters respectively set in voltmeter and ammeter position, respectively. In order to better calibrate the precision for the voltage and current values encountered in this experiment, we made a first discharge test of the 24 V<sub>DC</sub> batteries releasing into a 230 V<sub>AC</sub>-100 W incandescent lamp through a boost converter. The calibration process has resulted in the determination of the gain to be applied between the signals on the analog inputs and the displays on the computer screen (V<sub>umeter</sub>, digital displays) in accordance with those of the multimeters. Besides, this first experiment allowed us to discharge the battery bank to a level low enough to justify a realistic battery charging during long periods.

**Table 1 – Technical specifications of the CLIPSOL PV module.**

Type	Si-monocrystalline
Rated power ( $P_m$ )	175 W
Voltage at $P_m$ ( $V_m$ )	36.45 V
Current at $P_m$ ( $I_m$ )	4.81 A
Short-circuit current ( $I_{sc}$ )	5.1 A
Open-circuit voltage ( $V_{oc}$ )	43.7 V
Solar cells (number)	72, connected in series
Dimensions (mm)	1574 × 802 × 40

**Table 2 – Technical specifications of the MPPT/TSCC charge controller.**

Battery voltage	12/24 V Auto select
Maximum battery current	15 A
Maximum PV power <sup>a</sup> , 12/24 V	200/400 W (MPPT range 15/30 V –70 V)
Peak efficiency	98%
Self-consumption	10 mA
Charge voltage “absorption”	14.4/28.8 V
Charge voltage “float”	13.8/27.6 V
Charge algorithm	Multi-stage adaptive
Temperature compensation	–16/–32 mV/°C

<sup>a</sup> If more PV power is connected, the controller will limit input power to 200 W resp. 400 W.

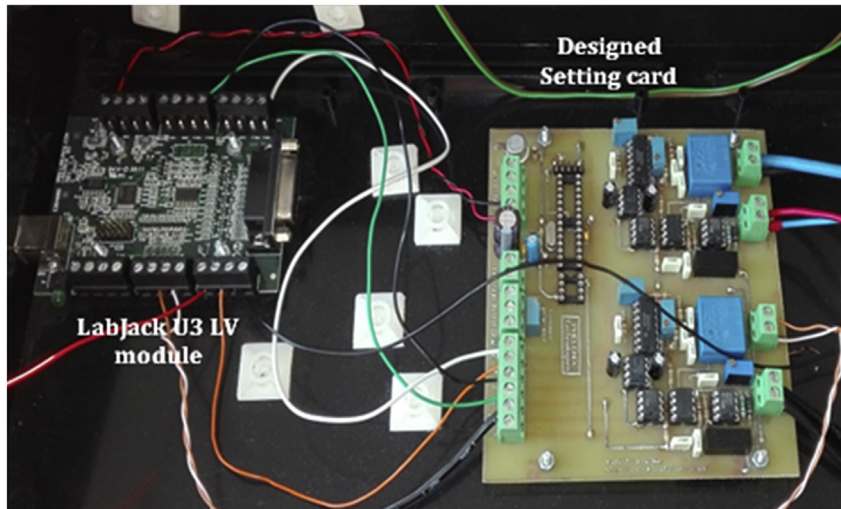


Fig. 2 – The data acquisition system.

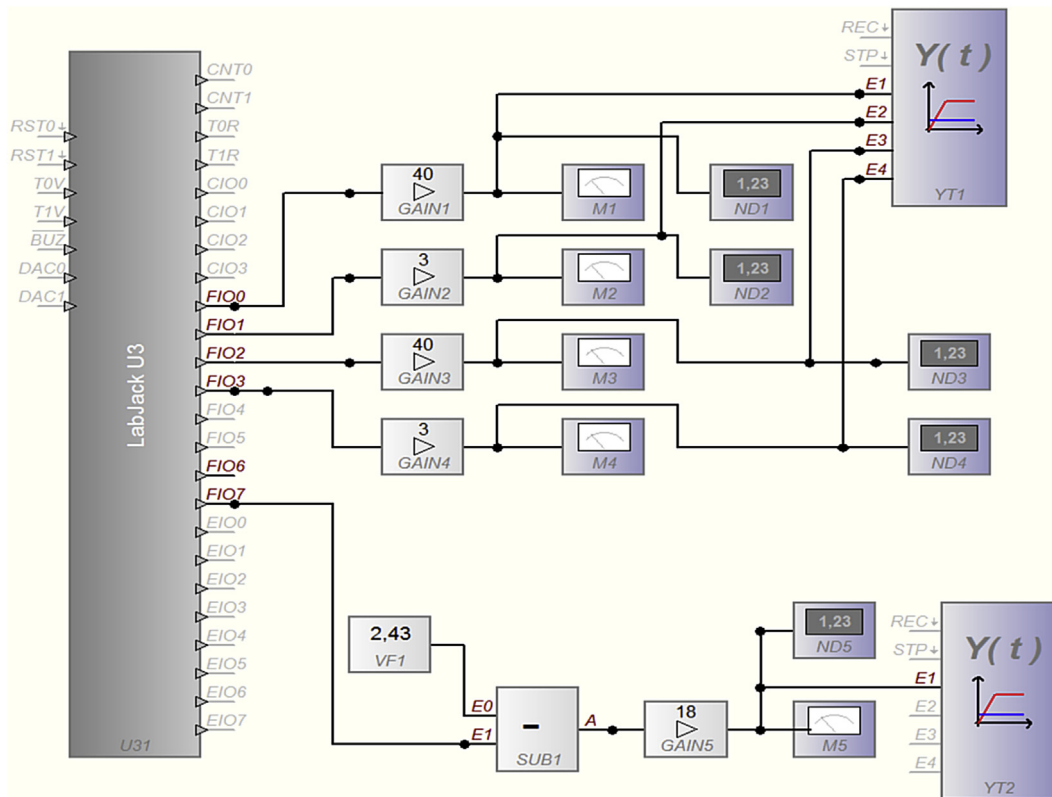


Fig. 3 – Function Block Diagram acquisition program under ProfiLab-Expert 4.0.

### Brightness appreciation

In order to have a correlation between the brightness level and the 24 V<sub>DC</sub> battery charging current, we have disposed, as reference, a 40 W monocrystalline PV module, of identical technology to that of the experiment, oriented and inclined in the same manner (~30°). As the short-circuit current is proportionate to the irradiation of the panel, we inserted a Hall effect sensor between this reference panel and an analog

input of the data acquisition system to measure the short-circuit current.

### Data acquisition and recording

Finally, there are five signals to be on view and to record, and as the ProfiLab-Expert 4.0 software allows only up to four signals in the same file simultaneously (namely the PV module and battery bank voltages and currents), the fifth signal

(the short-circuit current of the reference panel) is recorded in a second file.

A screenshot view of the graphical data acquisition control panel of the experiment is shown in Fig. 4. One can observe brightness fluctuations (short-circuit current) due to moving clouds during the experiment.

The numerical raw data is then saved into GRF file type (the default extension of ProfiLab-Expert 4.0 files) and data analysis is performed with Microsoft Excel.

### State of charge appraisal

Battery testing can be done in several ways which have been the subject of many researchers' works [29–33]. To truly measure the remaining capacity, one needs to perform the measurement of the density of the battery's electrolyte, i.e. to determine the specific gravity (SG) [26]. But this method is performed for open lead-acid batteries and not adapted for valve regulated lead acid batteries. A close second need is to simply look at the battery voltage level to get a rough indication of the battery's state of charge. The relationship between the battery voltage and the actual charge depends on the temperature and then, depending on the manufacturer, a correction factor should be applied (typically  $-0.03 \text{ V}/^\circ\text{C}$ ). It is important that when reading the battery voltage level, that it is not done during or right after it has been charged (or discharged), otherwise it will be relatively meaningless due to effects such as surface charge. To remove the surface charge from a freshly charged (or discharged) battery before testing, the battery should be left undisturbed for 12 h (no charging or

discharging) before a valid voltage measurement could be obtained [19,23–25].

There is a third method consisting in counting amp-hours (Ah) flowing in and out of the battery. This is the most convenient and accurate way to monitor a battery state of charge [30]. It is then necessary to use a battery monitor that is equipped with a sensor measuring the flowing current to perform the integration of the intensity over time [26]. However, calculating the available capacity can be complex because it depends on the discharge rate (Peukert effect) [24,27]. When a 12 V battery reaches 10.5 V, it is typically considered fully discharged [19,26].

## Charge control description

### The MPP tracking

The challenge for getting the best of a PV module is operating it at its Maximum Power Point (MPP), which corresponds to the peak power  $P_m$ , an essential parameter of the module, and optimal values  $I_m$  and  $V_m$  of the nominal current and voltage, Fig. 5.  $I_{sc}$  and  $V_{oc}$  are the Short-circuit current and the Open-circuit voltage of the PV module, respectively.

Indeed, the manufacturers always provide a PV module performance data under standard operating conditions STC (Standard Test Conditions). The STC may be considered in our latitudes ( $AM = 1.5$ , an incidence of  $41.8^\circ$ ) by a spring day or sunny autumn without mist, cold enough to keep the panel temperature at  $25^\circ\text{C}$ , or a day of great cold wind.

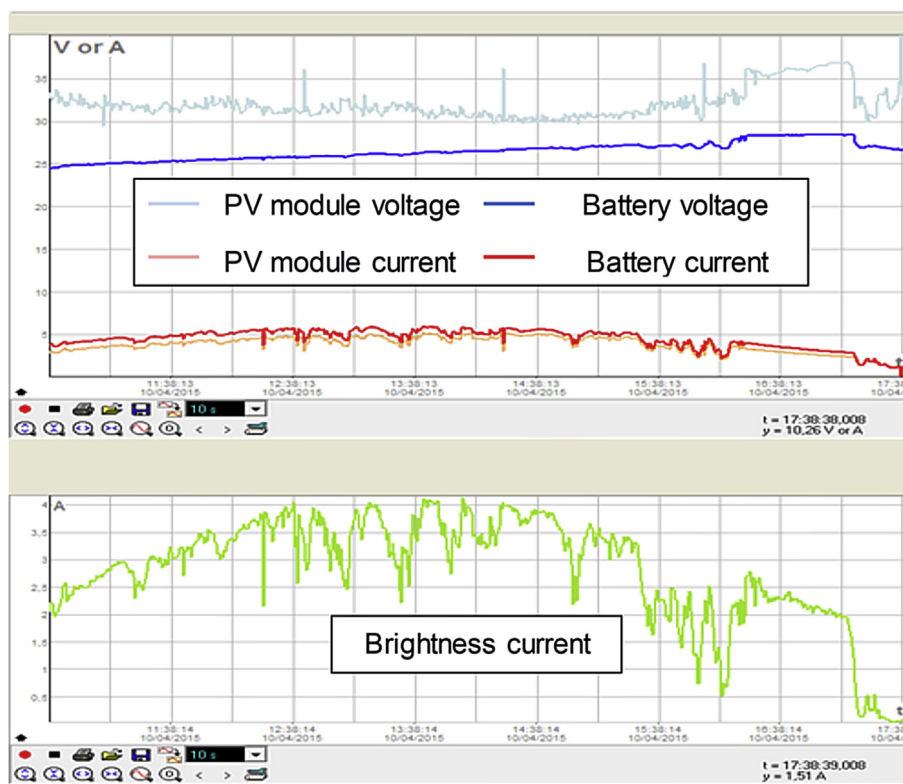


Fig. 4 – Real time graphical data acquisition control panel by ProfiLab-Expert 4.0.

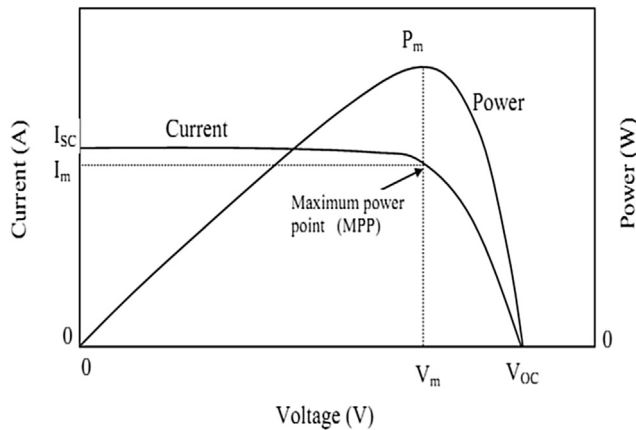


Fig. 5 – I–V and P–V characteristics of Solar panel.

However, most of the time the STC conditions cannot be met. Irradiance and temperature variations then affect the I–V characteristics, which mean a displacement of this MPP as shown in Fig. 6 [34].  $V_m$  slightly increases depending on the irradiance for the same temperature, but substantially decreases as a function of temperature for the same irradiance. Temperature and irradiance are bound in an unventilated panel (no wind): when the irradiance is high, the temperature of the panel increases inducing a decrease of  $V_m$  what, ultimately, drastically reduces the power [27,35].

One can note that the slight increase in current  $I_m$  following the temperature increase does not offset the drop of  $V_m$ .

The work of the MPP tracker is to lock onto this MPP regardless irradiance and temperature, therefore delivering to the load (battery bank in this case) the maximum of the produced power all the time. This controller works as a buck converter, so that it can ensure the charging of a battery by leaving the panel delivering a higher voltage than the latter, thanks to its power transistor controlled by a Pulse Width Modulation (PWM) microcontroller [35].

### The Three-Stage Charging Cycle

How to optimize the charging of a battery is independent of the power source, and depends only on the control device associated with it and the battery type (wet, AGM, gel) [19,23–26]. The recommended Three-Stage-Charging-Cycle, TSCC, performs as shown in Fig. 7. What differs, depending on the technology used, are the voltage values that determine the transition from one stage to another and the length of these stages. One must then consider manufacturers' specifications. Typical values of absorption and float charge voltage are given in Table 3, as an indication, for a temperature of 25 °C [24].

For the batteries used in this experiment, the given values are respectively 14.1V–14.4 V (20–25 °C) for Absorption, and 13.6V–13.8 V (15–25 °C) for floating [36], respectively and for the TSCC-MPPT Charge Controller these specific voltages are 14.4 V for Absorption and 13.8 V for Float [14], which matches with those of the batteries.

### Experimental measurements and analysis of energy exchanges

#### Preliminary estimate

For comparison thereafter, a preliminary estimate of an April mean day electrical energy production by the selected PV module is given in Table 4, considering the experimental conditions of the current date.

There, the local daily global irradiation the day of experiment is given by the French Institut National de l'Énergie Solaire (INES) [37]. The daily producible electrical energy and the rechargeable capacities are thus calculated as follows [35]:

$$E_{prod} = N_e \times P_p \quad (1)$$

where  $N_e = E_{sol}/1000$  (in h/day) is the number of equivalent hours, in which 1000 ( $W/m^2$ ) is the STC instantaneous irradiation;  $E_{sol}$  ( $kWh/m^2$ ) the daily global irradiation, and  $P_p$  (W) the peak power of the PV module.  $E_{prod}$  is the daily producible electrical energy (in Wh/day).

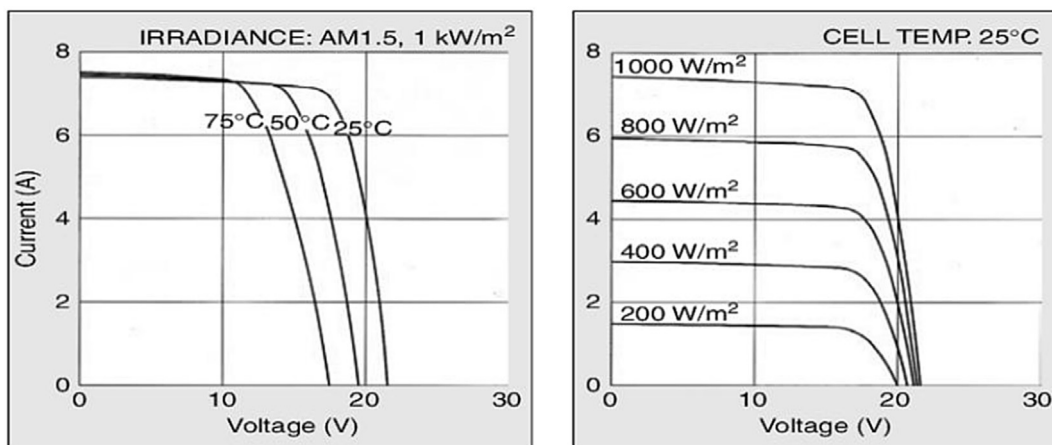


Fig. 6 – I–V characteristics under variable temperatures and irradiances for the Kyocera module KD135SX-UPU.

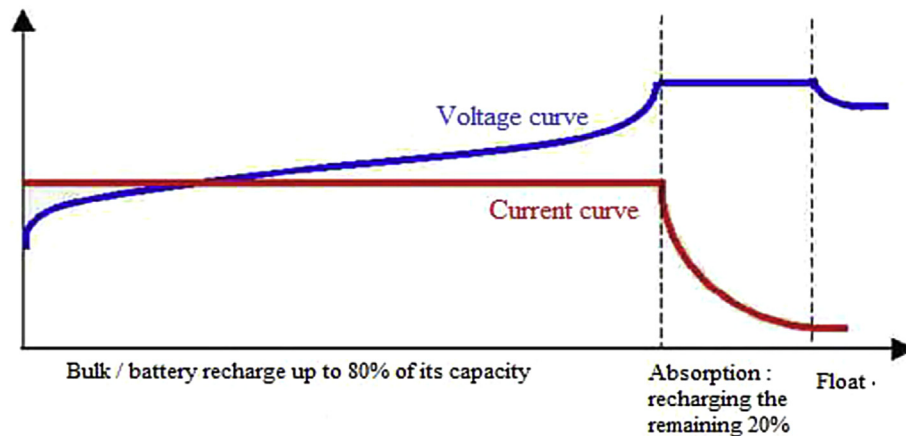


Fig. 7 – Typical Three-Stage Charging Cycle.

**Table 3 – Typical voltage limit values for charging control at 25 °C [11].**

Type of battery	Absorption voltage	Float voltage
Open lead	14.8 V	13.8 V
Sealed lead or AGM	14.4 V–14.6 V	13.0 V–13.8 V
Gel	14.1 V–14.4 V	13.3 V

**Table 4 – Assessment of the daily production of CLIPSOL PV module.**

Type	Monocrystalline
Rated power	175 W
Daily global irradiation	4.46 kWh/m <sup>2</sup>
Daily producible electrical energy	780.5 Wh
Battery nominal voltage	24 V
Charge controller efficiency	98%

#### Assessment of wiring losses

Since the experiment is conducted from an external pre-installed PV module, the wiring of the experimental installation is in two different sections of copper electrical cable: the existing wiring from the external PV module to the connection terminal; and the additional connection from the connection terminal to the battery bank. Table 5 summarizes the calculation of different ohmic losses in wiring.

Finally, the total wiring losses is found to be 15.65 Wh throughout the duration of the experiment, which, as will be seen subsequently, is 1.80% of the total PV module production.

#### Effective electrical energy generated by day

The theoretical estimation (Table 4) for a daily production is about 781 Wh. In fact, this assessment was done on the basis of the theoretical 4.46 daily number of equivalent hours. Fortunately, the day of this experiment the weather was so excellent that the PV module has produced for more than 7 h, at very high efficiency level. The computed results are summarized in Table 6. The electrical energy produced is deduced by integration over time of the measured PV voltage and current, considering wiring losses. One could observe in Fig. 8 that the best production period was between 11:30 AM and 3:30 PM this day, approximately corresponding to the indicated daily number of equivalent hours. During this period, the PV module performed above 70% of its peak power.

#### Effect of MPPT charge control

One can observe in Fig. 9 that the PV module voltage is all the time above the battery voltage, proof if any that the PV module performs at its MPP. The mean difference between PV module and battery voltages is 5.6 V, with a minimum of 2.85 V and a maximum of 13.5 V. Also, current ratio (PV module current by brightness current), which illustrates well the brightness dependence of the PV current, is almost constant throughout the day. Nevertheless, the MPPT charge controller brings up disturbances on the PV module current, which results in a fluctuation of the current ratio at the steps transitions Bulk/Absorption and Absorption/Float, and its sudden increase by the end of the charge cycle. In fact, the PV module is attempting to follow the command control law (charge controller is entering Absorption and Float modes), decreasing

**Table 5 – Ohmic losses in the wiring.**

Portion of cable	Cable length (m)	Cable section (mm <sup>2</sup> )	Ohmic resistance (mΩ)	Flowing through current	Lost energy (Wh)
PV module – Connection terminal	38.64	6	109.48	PV module current	11.73
Connection terminal – Charge controller	2.90	2.5	19.72	PV module current	2.11
Charge controller – Battery bank	1.80	2.5	12.24	Charge current	1.80



**Table 6 – PV module effective production.**

PV module Rated power	Estimated producible energy	Experiment period	Duration	PV module mean power	Mean value of power efficiency	Electrical Energy produced
175 W	780.5 Wh	10 h 38 min–17 h 41 min	7 h 03 min	123.55 W	70.60%	871.33 Wh

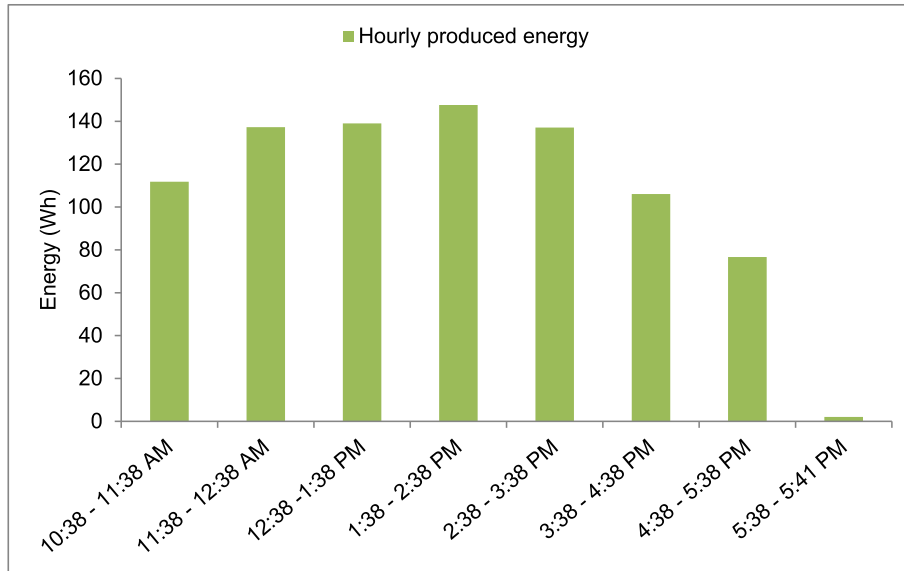


**Fig. 8 – Hourly produced energy of the PV module.**

the charge current. One can also remark that the PV module sometimes stands on open-circuit state within the Float step since the battery is fully charged.

**Electrical energy stored**

Charge current and battery voltage are measured over the battery bank and recorded all the day long so that the effective stored energy can be deducted. Fig. 10 shows the energy stored under the charge current. The effective stored energy rises to 835 Wh, about 95.80% of the PV module effective production. Of course, as for any physical system, the remainder of 4.20% is due to the installation losses.

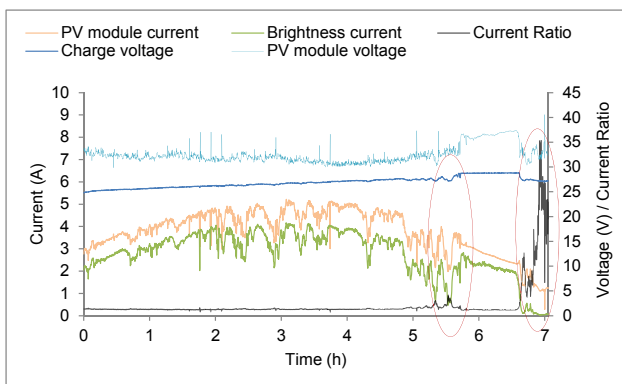


**Fig. 9 – Effect of MPPT charge control.**

**Balance sheet of charge conversion**

The difference between effective energies before and after the charge controller represents the charge conversion losses, either 21 Wh or 2.44%, approximately predictable when considering the manufacturer indicated efficiency 98% of our BlueSolar charge controller (referring to Table 7). In Fig. 11 one can observe that this very high level of efficiency (characterized by the power ratio) is reached during nearly all the charge cycle long, except by the end of the cycle, when the charge controller enters Float mode, and at the steps transitions.

**The battery bank parameters**

In battery storage technics, the stored electrical energy is expressed in terms of battery capacity and voltage to supply any electrical device. Fig. 12 shows the evolution of these two parameters during the various steps of the charge cycle.

When reading the final battery voltage in charging cycle, one would think that the 24 V battery bank is now recharged at 27.2 V. However, as reminded before, effective battery voltage is measured under open-circuit condition and at least 12 h after recharge; this was done the next day to find 25.6 V.

In practice, one often considers the relative quantity SOC, State of Charge of the battery, which indicates the available relative capacity for a standardized time of discharge (for the industry standard it is 20 h at 80 °F) until the voltage drops to 21 V. The initial and final parameters of the battery bank during this experience are then given Table 8.

Initial and final SOC are appraised using the manufacturer given capacity of 55 Ah and the open-circuit battery voltage.

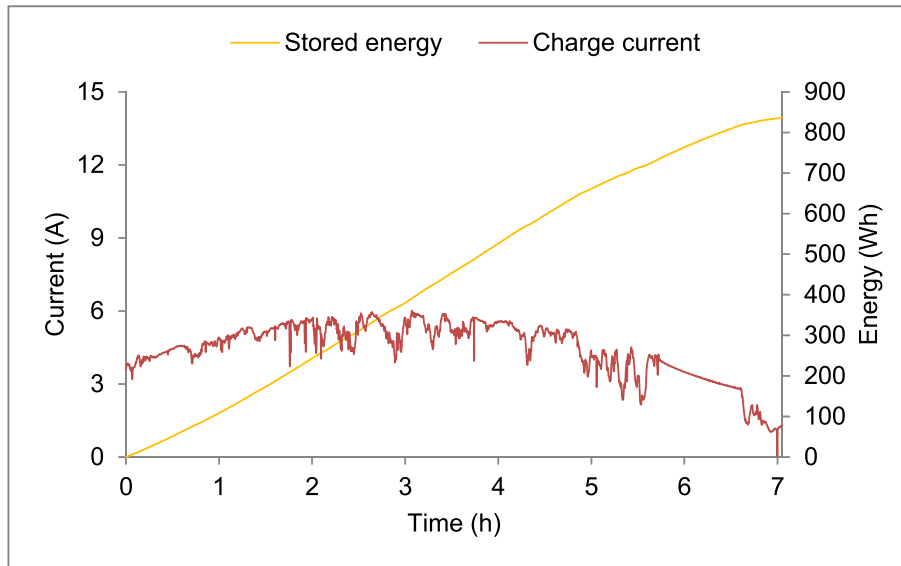


Fig. 10 – Stored energy and charge current.

Table 7 – Summary statement of energy exchanges.

PV energy produced	Wiring losses before charge controller	Wiring losses after charge controller	Battery bank's stored energy	Charge conversion losses	Charge conversion efficiency
871.4 Wh	13.9 Wh	1.80 Wh	834.8 Wh	20.9 Wh	97.56%
857.5 Wh		836.6 Wh			

## Experimental charging cycle analysis

### Charge control triggering

Prior to charging, the controller will detect voltage from the battery and then determines which stage to properly charge

at. Yet, the PV configuration must meet some prerequisites before charge cycle is triggered. For the MPPT charge controller used in the current PV configuration, its operating mode assumes that it will operate only if the PV output voltage exceeds the battery voltage ( $V_{bat}$ ), with a trigger PV voltage at minimum equal to  $V_{bat} + 5 V$  as starting voltage and a

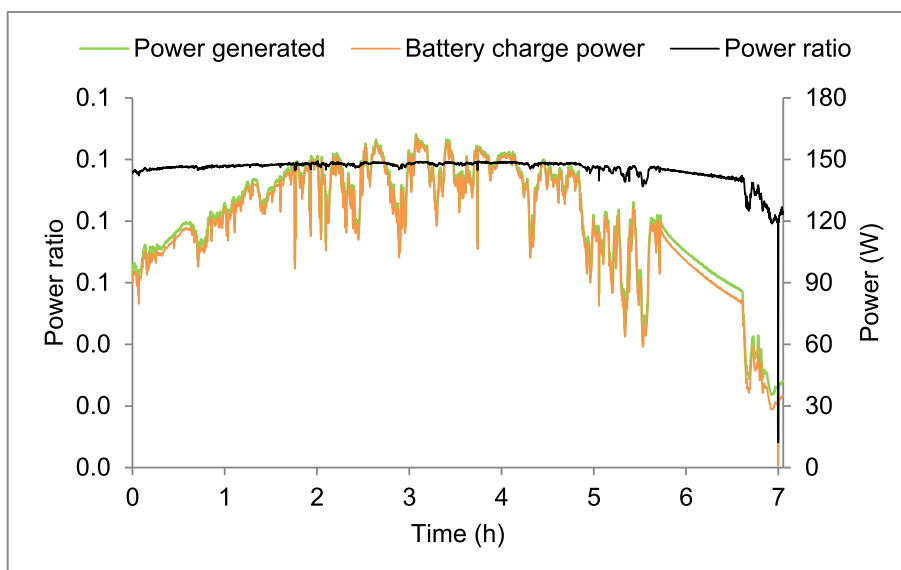


Fig. 11 – Conversion efficiency.

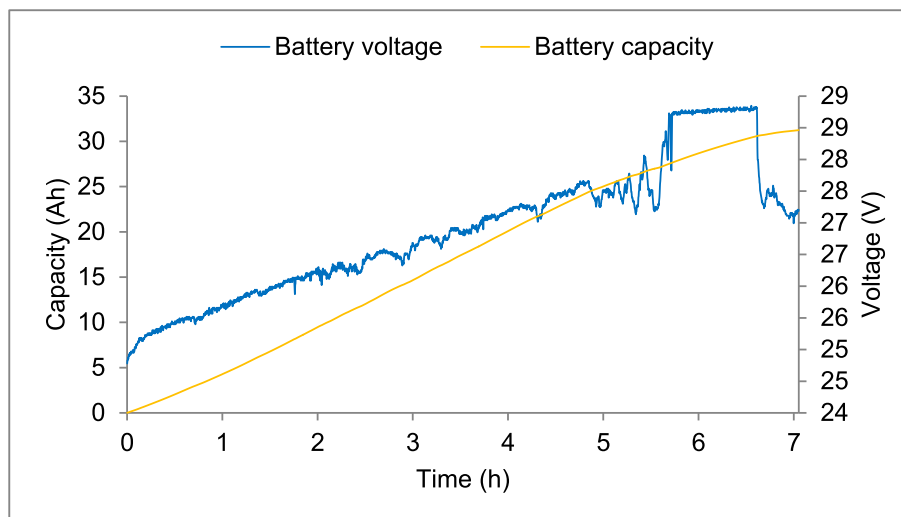


Fig. 12 – Battery bank's voltage and capacity during the charge cycle.

Table 8 – Battery bank's parameters.

Initial parameters		Refilled capacity/ Voltage increase	Final parameters	
Voltage	SOC	31.24 Ah/1.8 V	Voltage	SOC
23.8 V	~43%		25.6 V	100%

functioning PV voltage at a minimum equal to  $V_{bat} + 1$  V. By else, the maximum open-circuit PV voltage is 75 V [27].

Particularly for 24 V battery and mono- or polycrystalline panels, the minimum number of cells in series is 72 and the maximum is 108 cells. Such is the case in this experiment: the PV panel CLIPSOL-175 W is a monocrystalline of 72 cells in series; In Table 9, one can note that the initial PV voltage is 5 V higher than the initial battery voltage (33.9 V and 24.8 V respectively), and at least 1 V higher all the rest of the time. One can easily conclude the charge control has been operating throughout the whole experiment.

However, for a good precision of charge control, the maximum voltage drop for the Controller – Battery connection must not exceed 50 mV [35]. The voltage drop is due to the resistance of the wires and even if it stands between 12 mV and 74 mV as illustrated in Fig. 13, one can observe that within stages where accurate regulation is crucial for battery life and good recharge, absorption and float stages, this drop never reaches 50 mV.

### The three experimental stages

The TSCC-MPPT charge controller used in this experiment is configured for a Three-Stage Charging Cycle: Bulk – Absorption – Float. The above-mentioned (Table 2) stages for both charge voltages (28.8 V and 27.6 V respectively for Absorption and Float) allows us to distinguish these three stages as shown in Fig. 14, related to our experiment.

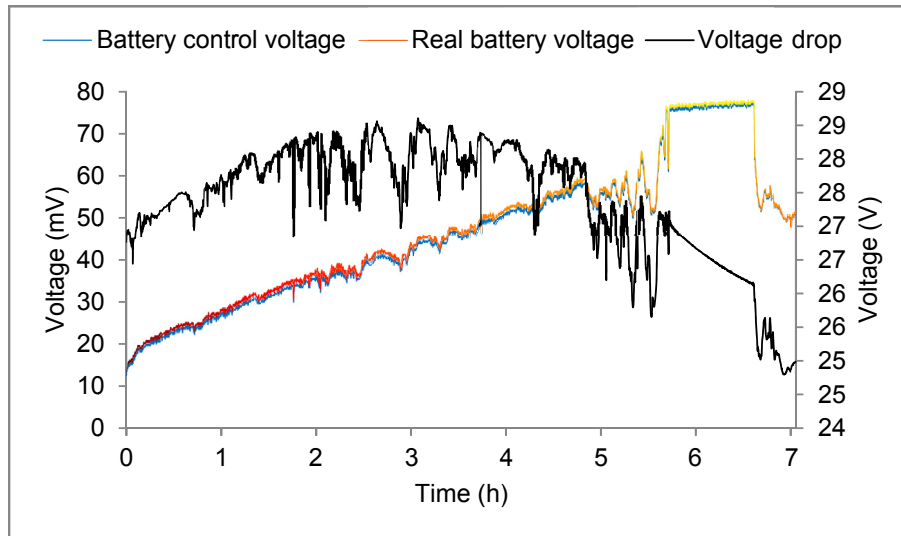
At first glance, the similitudes of charge current with the brightness current might suggest that it is proportional to brightness. The ratio illustrated in Fig. 15 shows well that it is

Table 9 – Synthesis of the charging cycle stages.

Charging steps	Bulk	Absorption	Float	Complete cycle
Duration	5 h 43 min 10 s	53 min 40 s	26 min 10 s	7 h 03 min
PV voltage: start-end	33.87 V–33.84 V	35.39 V–32.84 V	32.18 V–33.75 V	33.87 V–33.75 V
PV voltage range	30.04 V–37.29 V	32.84 V–37.44 V	30.37 V–35.46 V	30.04 V–37.44 V
Refunded capacity	27.63 Ah/53.1%	2.96 Ah/5.7%	0.65 Ah/1.3%	31.24 Ah/60.1%
Charge voltage: start-end	24.78 V–28.44 V	28.73 V–28.61 V	28.18 V–27.21 V	24.78 V–27.21 V
Charge voltage range	24.78 V–28.73 V	28.61 V–28.85 V	27.06 V–28.18 V	24.78 V–28.85 V
Average charge voltage value	26.55 V	28.77 V	27.33 V	26.88
Voltage STD <sup>a</sup>	0.79	0.03	0.20	1.03
Voltage CV <sup>b</sup>	2.99%	0.10%	0.72%	3.85%
Charge current: start-end	3.61 A–4.21 A	4.12 A–2.65 A	2.47 A–1.29 A	3.61 A–1.29 A
Charge current range	2.16 A–6.02 A	2.65 A–4.12 A	1.04 A–2.50 A	1.04 A–6.02 A
Average charge current value	4.83 A	3.30 A	1.50 A	4.43 A
Charge current STD <sup>a</sup>	0.73	0.35	0.36	1.13
Charge current CV <sup>b</sup>	15.13%	10.45%	23.71%	25.49%

<sup>a</sup> Standard deviation.

<sup>b</sup> Coefficient of variation.



**Fig. 13 – Control voltage drop.**

just the case in bulk stage, and evidently no more true (because of the PLW control of the charge controller) neither for absorption stage (regular decrease) nor for float stage (float current maintained at a low level).

The coefficient of variation is the ratio of the standard deviation to the average. It shows the extent of variability in relation to the means of measurements. It is calculated as follows:

$$CV = \frac{\sigma}{\bar{X}} * 100 \quad (2)$$

where  $\sigma$  is the standard deviation and  $\bar{X}$  the average.

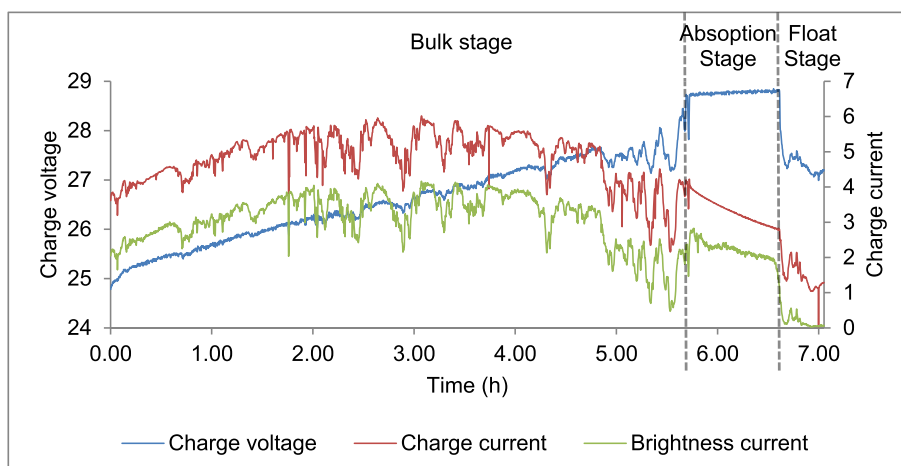
In this experiment, the Bulk stage lasts for 5 h and 43 min during which the controller delivers as much current as possible to rapidly recharge the battery bank. The delivered current is higher than the one the controller receives from the PV module (Fig. 4) because, at a given Maximum Power Point, the lowering of voltage realized by the buck function of the controller conducts to a substantial increase of the charge current. Bulk current is relatively variable, CV = 15.13% (see

Table 9), since it varies over brightness fluctuations due to moving clouds during the experiment and the path of the sun with a maximum at solar noon (2 PM in summer).

On this Bulk step, charge current has reached its maximal value 6.02 A, and the mean value of current (4.83 A, less than C/10) is the highest of the three stages mean values. 27.63 Ah has been then refunded to the battery bank, representing 88.44% of the complete refilled capacity. Considering the estimated initial SOC of around 43% (see Table 9), one can conclude that “bulk step” has effectively refunded the batteries bank at a higher SOC than the predicted 80%.

For the Absorption stage, it lasts about 53 min and nearly 3 Ah had been refunded to the battery bank. The battery voltage is held quasi-steady at 28.8 V, hardly fluctuating (CV = 0.10%), while the charge current is continuously declining from 4.12 A to 2.65 A. This stage takes much longer when compared to the first 3 Ah during the bulk stage, where just 42 min were long enough.

Float stage starts at nearly 99% of the state of charge. It brings the battery all the way through and maintains the 100%



**Fig. 14 – Experimental Three-Stage Charging Cycle.**

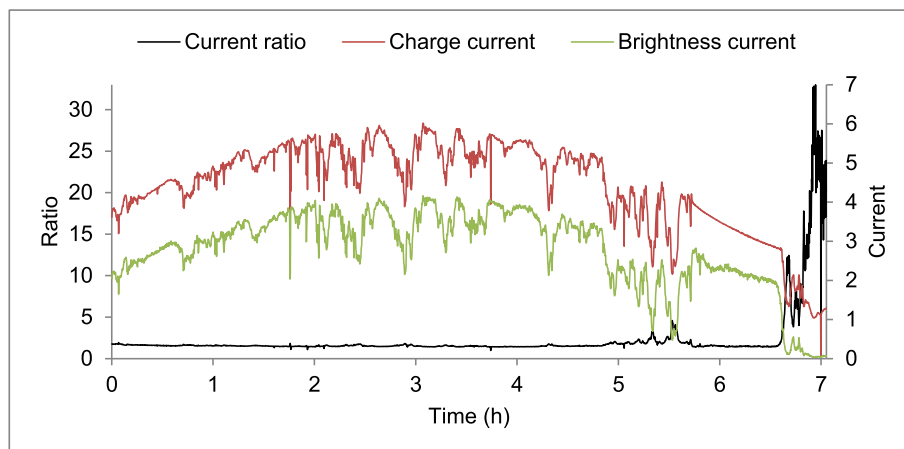


Fig. 15 – Brightness/Charge current ratio.

state of charge. During this step, the charge current decreased down to 1.3 A with a CV of 23.7%, the highest one, very well illustrating the regulation by the controller to maintain the battery in a fully charged state, as it could be observed in Figs. 14 and 15.

The experience is then voluntarily stopped because the float period is judged long enough (26 min) to be considered as stable.

In the current work, we addressed the daily storage and other aspects than the quality and the optimization of load should be taken into account when selecting the storage system. In particular, investment cost and environmental constraints such as, ambient temperature, storage and maintenance have to be considered. These parameters directly influence the efficiency of the batteries. Considering existing storage systems, a comparison between lead-acid and hydrogen storage is not really relevant as the hydrogen storage solution addresses seasonal storage (between summer and winter). Otherwise, considering the second type of current storage solution based on Li-ion technology, despite a higher energy density and a better autonomy compared to lead-acid batteries, their huge initial cost drastically limit their integration in PV off-grid systems. Additionally, considering the particularities of the photovoltaic source, our study points out that a special attention paid to the quality of the battery charge process offers the possibility of pushing back the technological barriers of lead batteries influencing their safety, longevity and performance. Thus, lead-acid battery solution can continue to be a preferred storage solution for off-grid PV systems.

## Conclusion

Whether for the battery bank itself or for the electrical energy supply, the experts in the field of off-grid PV systems all agree to say that the success key of such systems remains the regulation of battery charging. In this experiment, the PV module has been operating all day at a very high performance level (over 70% on average), reaching up to 95% sometimes. This efficiency is the result of the charge controller MPP

tracking, and this is proven through the PV module voltage, which remained above battery voltage all the time, with a mean difference over 5 V. As for the Three-Stage Charging Cycle, its function is verified in this experiment as we can well observe the adaptation of charging speeds (fast charge in Bulk stage with elevation of the PV module current, moderate and stable in Absorption stage). These operation characteristics are essential both for the health and for the quality of charge of batteries used as storage in a PV energy system. Thus, considering the particularities of the photovoltaic source, our study points out that a special attention paid to the quality of the battery charge process offers the possibility of pushing back the technological barriers of lead batteries influencing their safety, longevity and performance and lead-acid battery solution can continue to be a preferred storage solution for off-grid PV systems.

## Acknowledgments

We are grateful to Jean-Pierre Charles, Emeritus Professor, Université de Lorraine (France) for his essential participation and assistance in some parts of this project and we thank Abdoul Aziz Bogno, University of Alberta (Canada), for his specific contribution in the finalisation of the publication.

## REFERENCES

- [1] Della RM, Rand DAJ. Energy storage – a key technology for global energy sustainability. *J Power Sources* 2001;100. [http://dx.doi.org/10.1016/S0378-7753\(01\)00894-1](http://dx.doi.org/10.1016/S0378-7753(01)00894-1) [Elsevier].
- [2] Belmonte N, Girgenti V, Florian P, Peano C, Luetto C, Rizzi P, et al. A comparison of energy storage from renewable sources through batteries and fuel cells: a case study in Turin, Italy. *Int J Hydrogen Energy* 2016;41(46):21427–38. <http://dx.doi.org/10.1016/j.ijhydene.2016.07.260>.
- [3] Ibrahim H, Ilinca A, Perron J. Energy storage systems: characteristics and comparisons. *Renew Sust Energy Rev* 2008;12:1221–50. <http://dx.doi.org/10.1016/j.rser.2007.01.023>.
- [4] Dunn B, Kamath H, Tarascon JM. Electrical energy storage for the grid: a battery of choices. *Science* 2011;334:928–35.

- [5] Zilles R, Lorenzo E, Serpa R. From candles to PV electricity: a four-year experience at Iguape-Cananeia, Brazil. *Prog Photovolt Res Appl* 2000;8:421–34.
- [6] Huacuz JM, Flores R, Agredano J, Munguia G. Field performance of lead–acid batteries in photovoltaic rural electrification kits. *Sol Energy* 1995;55(4):287–99. [http://dx.doi.org/10.1016/0038-092X\(95\)00047-U](http://dx.doi.org/10.1016/0038-092X(95)00047-U).
- [7] Mohammadi A, Rekioua D, Rekioua T, Bacha S. Valve Regulated Lead Acid battery behavior in a renewable energy system under an ideal Mediterranean climate. *Int J Hydrogen Energy* 2016;41(45):20928–38. <http://dx.doi.org/10.1016/j.ijhydene.2016.05.087>.
- [8] Bogno B, Mohammadou S, Aillerie M. Technical and economic sizing of the energy storage in an autonomous hybrid power generator for rural electrification in sub-equatorial area of Africa. *Energy Procedia* 2015;74:707–17. <http://dx.doi.org/10.1016/j.egypro.2015.07.806> [Elsevier].
- [9] Ganeshan IS, Manikandan VVS, Sundhar VR, Savji R, Shanthi C, Kottayil SK, et al. Regulated hydrogen production using solar powered electrolyser. *Int J Hydrogen Energy* 2016;41:10322–6. <http://dx.doi.org/10.1016/j.ijhydene.2015.05.048>.
- [10] Ursua A, Barrios EL, Pascual J, San Martin I, Sanchis P. Integration of commercial alkaline water electrolyzers with renewable energies: limitations and improvements. *Int J Hydrogen Energy* 2016;41:12852–61. <http://dx.doi.org/10.1016/j.ijhydene.2016.06.071>.
- [11] Lavorante MJ, Messina LG, Franco JI, Bonelli P. Design of an integrated power system using a proton exchange membrane fuel cell. *Int J Hydrogen Energy* 2014;39:8631–4. <http://dx.doi.org/10.1016/j.ijhydene.2013.12.071>.
- [12] Madaci B, Chenni R, Kurt E, Hemsas KE. Design and control of a stand-alone hybrid power system. *Int J Hydrogen Energy* 2016;41:12485–96. <http://dx.doi.org/10.1016/j.ijhydene.2016.01.117>.
- [13] Bayrak ZU, Bayrak G, Ozdemir MT, Gencoglu MT, Cebeci M. A low-cost power management system design for residential hydrogen & solar energy based power plants. *Int J Hydrogen Energy* 2016;41:12569–81. <http://dx.doi.org/10.1016/j.ijhydene.2016.01.093>.
- [14] Dufo-Lopez R, Lujano-Rojas JM, Bernal-Agustin JL. Comparison of different lead-acid battery lifetime prediction models for use in simulation of stand-alone photovoltaic systems. *Appl Energy* 2014;115:242–53. <http://dx.doi.org/10.1016/j.apenergy.2013.11.021>.
- [15] Kabakian V, McManus MC, Harajli H. Attributional life cycle assessment of mounted 1.8 kWp monocrystalline photovoltaic system with batteries and comparison with fossil energy production system. *Appl Energy* 2015;154:428–37. <http://dx.doi.org/10.1016/j.apenergy.2015.04.125>.
- [16] Bogno B, Mohammadou S, Aillerie M. Technical and economic analysis of a wind power generation system for rural electrification in subequatorial area of Africa. *Energy Procedia* 2014;50:773–81. <http://dx.doi.org/10.1016/j.egypro.2014.06.095> [Elsevier].
- [17] Jossen A, Garcke J, Sauer DU. Operation conditions of batteries in PV applications. *Sol Energy* 2004;76(6):759–69. <http://dx.doi.org/10.1016/j.solener.2003.12.013>.
- [18] Díaz P, Egido MA. Experimental analysis of battery charge regulation in photovoltaic systems. *Prog Photovolt Res Appl* 2003;11(7):481–93. <http://dx.doi.org/10.1002/pip.509>.
- [19] Battery Charging Tutorial website. Available at: <http://www.chargingchargers.com>. [Accessed on June 2016].
- [20] Kim JM, Song SB, Jung JS, Lee MS, Golovanov D, Baek G, et al. Battery charging method and battery pack using the same. U.S. Patent Application 15/006,883, filed January 26, 2016.
- [21] Eldahab YEA, Saad NH, Zekry A. Enhancing the design of battery charging controllers for photovoltaic systems. *Renew Sustain Energy Rev* 2016;58:646–55. <http://dx.doi.org/10.1016/j.rser.2015.12.061>.
- [22] Koutroulis E, Kalaitzakis K. Novel battery charging regulation system for photovoltaic applications. *IEE Proc Electric Power Appl* 2004;151(2):191–7.
- [23] Chargetek, Inc. website. Available at: <http://www.chargetek.com>. [Accessed on June 2016].
- [24] Seatronic website. Available at: <http://conseil.seatronic.fr/index.php>. [Accessed on June 2016].
- [25] Solar Power Planet Earth website. Available at: <http://www.solarpowerplanetearth.com/index.html>. [Accessed on June 2016].
- [26] Vader R. *Energy unlimited. Victron Energy B.V; June 2011.*
- [27] BlueSolar charge controller MPPT 70/15. Technical instructions manual. Victron Energy.
- [28] ProfiLab-Expert 4.0. Available at: <http://profilab-expert.software.informer.com/4.0/>. [Accessed on April 2016].
- [29] Gonzalez I, Ramiro A, Calderon M, Calderon AJ, Gonzalez JF. Estimation of the state-of-charge of gel lead-acid batteries and application to the control of a stand-alone wind-solar test-bed with hydrogen support. *Int J Hydrogen Energy* 2012;37(15):11090–103. <http://dx.doi.org/10.1016/j.ijhydene.2012.05.001>.
- [30] Piller S, Perrin M, Jossen A. Method for state-of-charge determination and their applications. *J Power Sources* 2001;96:113–20. [http://dx.doi.org/10.1016/S0378-7753\(01\)00560-2](http://dx.doi.org/10.1016/S0378-7753(01)00560-2).
- [31] Zhang J, Xia Ch. State-of-charge estimation of valve regulated lead acid battery on multi-state unscented Kalman filter. *Int J Electr Power Energy Syst* 2011;33:472–6.
- [32] Ng KS, Moo Ch-S, Chen YP, Hsieh Y-Ch. Enhanced coulomb counting method for estimating state-of-charge and state-of-health of lithium-ion batteries. *Appl Energy* 2009;86:1506–11. <http://dx.doi.org/10.1016/j.apenergy.2008.11.021>.
- [33] Cadirci Y, Ozkazanc Y. Microcontroller-based on-line state-of-charge estimator for sealed lead-acid batteries. *J Power Sources* 2004;129:330–42. <http://dx.doi.org/10.1016/j.jpowsour.2003.11.008>.
- [34] KYOCERA Solar, Inc. website. Available at: <http://www.kyocerasolar.com>. [Accessed on June 2016].
- [35] Labouret A, Viloz M. *Energie Solaire Photovoltaïque. 3e edition. Dunod; 2006.*
- [36] DAB12-55-SOL. Maintenance free AGM batteries. Solar batteries technical datasheet.
- [37] Institut National de l'Energie Solaire, INES website. Available at: <http://ines.solaire.free.fr>. [Accessed on April 2016].